The Use of New PHACOMP in Understanding the Solidification Microstructure of Nickel Base Alloy Weld Metal

M. J. CIESLAK, G. A. KNOROVSKY, T. J. HEADLEY, and A. D. ROMIG, Jr.

The weld metal microstructures of five commercial nickel base alloys (HASTELLOYS* C-4, C-22, and C-276, and INCONELS* 625 and 718) have been examined by electron probe microanalysis and analytical electron microscopy. It has been found that solidification terminates in many of these alloys with the formation of a constituent containing a topologically-close-packed (TCP) intermetallic phase (*i.e.*, σ, P, Laves). Electron microprobe examination of gas-tungsten-arc welds revealed a solidification segregation pattern of Ni depletion and solute enrichment in interdendritic volumes. New PHACOMP calculations performed on these segregation profiles revealed a pattern of increasing M_d (metal-*d* levels) in traversing from a dendrite core to an adjacent interdendritic volume. In alloys forming a terminal solidification TCP constituent, the calculated M_d values in interdendritic regions were greater than the critical M_d values for formation of σ as stated by Morinaga *et al.* Implications of the correlation between TCP phase formation and M_d in the prediction of weld metal solidification microstructure, prediction of potential hot-cracking behavior, and applications in future alloy design endeavors are discussed.

I. INTRODUCTION

SOLIDIFICATION during arc welding is an inherently nonequilibrium process. Microstructures generated during arc welding are often not those predicted by applying equilibrium considerations to existing phase diagrams. In some cases, such as the Al-Mg system, the formation of a relatively large volume fraction of a nonequilibrium eutectic constituent makes possible the fabrication of readily weldable alloys such as 5456 (Al-5.2 wt pct Mg). Usually, though, the formation of a low-melting nonequilibrium eutectic constituent is detrimental from a weld hot-cracking viewpoint.

The sequence of solidification reactions in commercial alloys is of prime importance in diagnosing not only hot-cracking propensity but also in understanding subsequent solid-state transformations and materials properties derived from these transformations. Unfortunately, phase diagrams are lacking for virtually every alloy system incorporating more than three components and are generally limited in scope even for ternary systems.

In the case of nickel base alloys, much fundamental and empirical effort has gone into describing phase relationships in the solid state. Nickel base alloys are generally derived from at least ternary systems and more usually quaternary or higher order systems. The face-centered-cubic Ni matrix has a high solubility for many substitutional alloying elements, but commercial alloys often contain a large number of minor phases (carbides, nitrides, borides, intermetallic compounds, *etc.*). The occurrence of certain topologically-close-packed (TCP) intermetallic phases, such as μ, σ, and Laves, has been shown to influence the mechanical properties of nickel and cobalt base superalloys.[1-4] As phase diagrams were not available for complex systems, metallurgists compiled empirical data on the occurrence of these phases in commercial alloys. In the 1950's, several authors[5-9] investigating binary and ternary alloy systems applied the electron vacancy concept of Pauling[10] and realized that σ phase was an electron compound,[11] the presence of which could be predicted in other alloy systems.

Later, Woodyatt, Sims, and Beattie[12] advanced this predictive capability to complex, commercial alloys through a calculation scheme known by the acronym PHACOMP (for PHAse COMPutation). The average electron hole number, defined as N_v, for the austenitic matrix is calculated after accounting for the formation of all phases normally encountered in nickel base superalloys (carbides, γ', borides, *etc.*). The algebraic definition of N_v is given as follows:

$$N_v = \sum(x_i)\,(n_v^i) \qquad [1]$$

where x_i is the atomic fraction of element i and n_v^i is the electron hole number of element i. Table I lists values of n_v^i for the common elements found in nickel-base alloys. A critical electron hole number, based upon studies of binary and ternary alloy systems and upon the collected empirical data from vast numbers of heats of commercial alloys, was established as the "σ-safe" boundary. That is, when the critical value of N_v was exceeded in the residual austenitic matrix, σ would be predicted to form. In a similar manner, "μ-safe" and "Laves-safe" boundaries have been established.[13] By using this approach, alloy design and chemistry control have been carried out for the past two decades.

It must be pointed out, though, that problems have arisen in predicting the "safe" compositions for some alloys, such as Alloy 713-C.[3,14] In addition, calculational difficulties have been ascribed to alloys having relatively high Mo or W contents. In general, elements not located in the first long row (transition metals) of the Periodic Table have been simply assigned individual n_v numbers equal to those of the elements at the top of their respective columns. Subsequent attempts to correlate these values with ternary phase diagram data has resulted in, for example, the assigning

*HASTELLOY is a trademark of Cabot Corporation. INCONEL is a trademark of the INCO family of companies.

M. J. CIESLAK and G. A. KNOROVSKY, Org. 1833, Process Metallurgy, T. J. HEADLEY, Org. 1822, Electron Optics and X-ray Analysis, and A. D. ROMIG, Jr., Org. 1832, Physical Metallurgy, are with Sandia National Laboratories, P.O. Box 5800, Albuquerque, NM 87185.

Manuscript submitted March 14, 1986.

of n_v^{Mo} numbers from 4.66 to 10.[15] A more sophisticated PHACOMP technique, which defines temperature dependent critical N_v values, has also been suggested.[16]

Recently, a more fundamental and elegant approach to the problem of austenite phase stability *vs* TCP phase (and other intermetallic phases) -formation in nickel base alloys has been developed by Morinaga *et al.*[17,18] With a quantum mechanical calculational technique, the DV-Xα (discrete variational cluster) method, a different type of PHACOMP, called New PHACOMP, was developed. Instead of calculating an average electron hole number, the average *d*-electron energy above the Fermi level is calculated for the same residual austenitic matrix. This average *d*-electron energy is called M_d and is defined algebraically as:

$$M_d = \sum(x_i)(m_d^i) \quad [2]$$

where x_i is the atomic fraction of element i and m_d^i is the metal *d*-level of element i. Elemental values of m_d^i are given in Table I. In a manner analogous to the original PHACOMP, New PHACOMP calculations are used to predict the occurrence of intermetallic phases such as TCP phases in a nickel-base austenitic matrix. Temperature dependent critical values of M_d, calculated from appropriate binary and ternary phase diagrams, were established for "σ-safe" alloys such that when these values were exceeded, σ would be expected to occur. In addition, other phase boundaries ($\gamma/\gamma + \beta$(NiAl), $\gamma/\gamma + \gamma'$, and $\gamma/\gamma + \mu$) were also predicted by specific critical M_d values. In particular, the temperature-dependent "σ-safe" expression is given as:[17]

$$M_d^{crit} = 6.25 \times 10^{-5} T + 0.834 \quad [3]$$

where T is the absolute temperature in Kelvin.

A method for predicting phase stability, microstructure, and solidification sequence in austenitic stainless steel weld metal has also been developed,[19-22] based upon a Cr and Ni equivalent concept. It has been determined that alloying elements normally found in stainless steels have similar phase stabilizing behavior as either Cr or Ni. Those elements which act in a manner similar to Cr (Mo, Si, Ti, Nb, W, Ta, V, Al) tend to stabilize the body-centered-cubic ferritic phase. Elements which behave similarly to Ni (C, N, Mn, Cu, Co) tend to stabilize the face-centered-cubic austenitic phase. An excellent historical review of this development has been recently published by Olson.[22] In an analogous manner, an equivalent composition model has recently been proposed by Cieslak *et al.*[23,24] to describe the solidification and solid state transformation microstructure in austenitic Ni-Cr-Mo-Fe-W weld metals.

It must be remembered that the entire history of the development of PHACOMP-type calculations for austenitic superalloys and equivalency models for austenitic weld metals has been driven by the desire to establish the γ solvus *vs* a variety of other possible phases in complex, multicomponent systems for which phase diagrams are not available. The purpose of this study is to show that a correlation exists between the weld solidification microstructure in the nickel base alloys investigated and critical values of the M_d parameter from the New PHACOMP formalism.[17]

Table I. Elemental n_v and m_d Values

Element	n_v^i	m_d^i
Ti	6.66	2.271
V	5.66	1.543
Cr	4.66	1.142
Mn	3.66	0.957
Fe	2.66	0.858
Co	1.71	0.777
Ni	0.66	0.717
Zr	6.66	2.944
Nb	5.66	2.117
Mo	4.66	1.550
Ta	5.66	2.224
W	4.66	1.655
Al	7.66	1.900
Si	6.66	1.900

II. EXPERIMENTAL PROCEDURE

The mill analyses of the alloys used in this investigation are given in Table II. All alloys tested were in the mill annealed condition prior to welding. All welding was done using the autogenous (no filler metal added) gas-tungsten-arc (GTA) process, direct current, electrode negative. Welds were made using a current of 100 amperes at a travel speed of 20 cm/min (90 amperes at 22 cm/min for INCONEL 718). Argon was the shielding gas.

The weld metal analyzed was obtained from Varestraint Test[25,26] (a fusion zone hot-cracking test) specimens. Weld metal analysis involved scanning electron microscopy (Hitachi S-520), electron probe microanalysis (Cameca MBX), and transmission electron microscopy (JEOL 100C).

After welding, samples for bulk microstructural analysis were sectioned from Varestraint specimens and included the fusion zone hot cracks present. The samples were mounted in epoxy and polished through 0.05 μm alumina. The microstructures were revealed by a 10 pct chromic acid electroetch. Those specimens to be examined in the scanning electron microscope (SEM) were carbon coated prior to examination.

The specimens for electron probe microanalysis had microhardness indentations placed on the specimen surface to bracket areas for analysis. The etched surfaces were then repolished flat with 1 μm diamond paste and carbon coated prior to analysis. Profiles were taken across weld metal dendrites perpendicular to the dendrite growth direction. Care was taken to avoid interdendritic constituents during profiling. The microprobe was operated at an accelerating potential of 15 kV and a beam current of approximately 20 nA. K_α X-ray peaks were used to analyze for all elements of interest except for Mo, W, and Nb, where the L_α peaks were used. Point count data were reduced to weight percentages with a $\phi(\rho, Z)$ computer algorithm.[27]

Samples for transmission electron microscopy were sliced from the weld metal of Varestraint specimens with a low-speed carbide saw and ground to a thickness of approximately 125 μm. Standard 3 mm-diameter disks were cut from the thin sheet with a mechanical punch. Thin foils were prepared by electropolishing in a solution of 10 pct perchloric acid in methanol at approximately −65 °C. Following electrochemical thinning, the foils were placed in an ion

mill to increase the amount of thin area and to remove any electrolyte residue. The foils were examined in a JEOL 100C AEM operated at 100 kV. Selected-area electron diffraction was used to uniquely identify phases in the weld metals' microstructures.

III. RESULTS

A. *Microstructural Analysis*

Figures 1 through 5 are SEM secondary electron photomicrographs of the weld metal microstructures of the five alloys studied. In all cases fusion zone hot cracks are present in the figures and terminal solidification constituents can be seen (except in Figure 1, HASTELLOY C-4) associated with the hot cracks. In general, it was observed that INCONEL 718 had the largest volume fraction of terminal solidification constituent, and that HASTELLOY C-4 had the least (none observable in the SEM).

Higher magnification SEM analysis revealed a lamellar, eutectic-like morphology of these terminal solidification constituents. Figure 6 shows this well-developed structure in INCONEL 718 weld metal. A similar morphology can be seen in Figure 7 for INCONEL 625 weld metal. HASTELLOYS C-22 (Figure 8) and C-276 (Figure 9) have a somewhat less well-developed structure, probably the result of a lower volume fraction of terminal solidification constituent in these two alloys.

Electron diffraction experiments performed on these alloys revealed the crystal structure of the terminal solidification constituents. In both INCONELS 625 and 718, the predominant terminal solidification constituent contains a Nb-rich Laves phase (hexagonal, a = 0.479 nm, c = 0.770 nm). Some NbC/austenite terminal solidification constituent is also observed, especially in INCONEL 718. In HASTELLOY C-22, the terminal solidification phase is

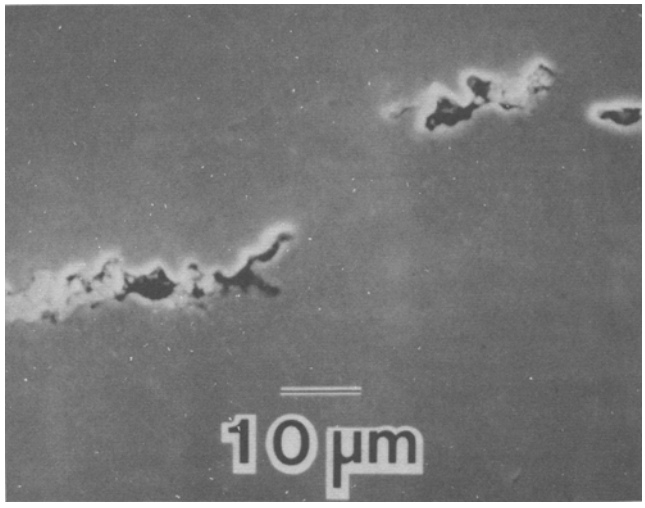

Fig. 1—SEM micrograph of weld hot-cracked region in HASTELLOY C-4.

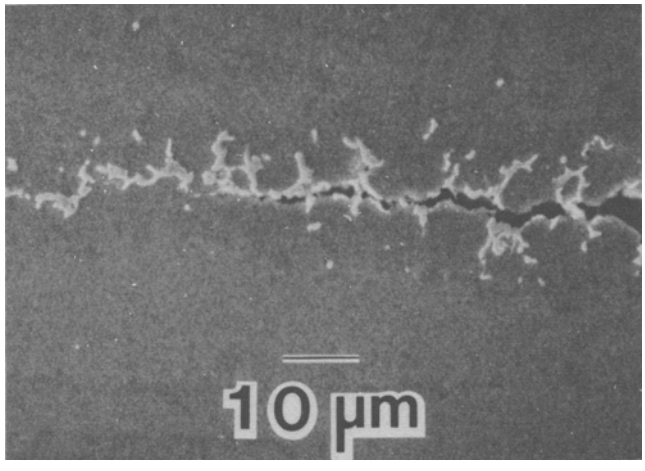

Fig. 2—SEM micrograph of weld hot-cracked region in HASTELLOY C-22.

Table II. Alloy Compositions*

Element	HASTELLOY C-4	HASTELLOY C-22	HASTELLOY C-276	INCONEL 625	INCONEL 718
Al	0.33	0.30	0.30	0.41	0.56
B	<0.002	—	<0.002	0.0012	0.002
C	0.004	0.006	0.003	0.01	0.04
Co	0.10	0.84	0.96	—	0.11
Cr	15.69	21.22	15.83	20.43	18.18
Cu	0.02	0.08	0.16	0.01	0.15
Fe	0.45	3.17	5.44	3.64	18.10
Mg	0.010	—	0.025	—	—
Mn	0.17	0.31	0.50	0.06	0.13
Mo	15.06	13.43	15.56	8.71	3.12
N	—	0.041	0.017	—	—
Nb	—	<0.04	—	3.49	5.25
Ni	67.20	56.96	55.58	62.77	53.20
P	<0.005	0.010	0.014	0.013	0.014
S	<0.002	<0.002	0.002	0.003	0.002
Si	0.03	<0.02	0.03	0.06	0.21
Ta	—	0.06	—	—	—
Ti	0.23	0.03	<0.01	0.27	0.95
V	0.02	0.14	0.18	—	—
W	<0.10	3.29	3.93	—	—

*All concentrations in weight percent

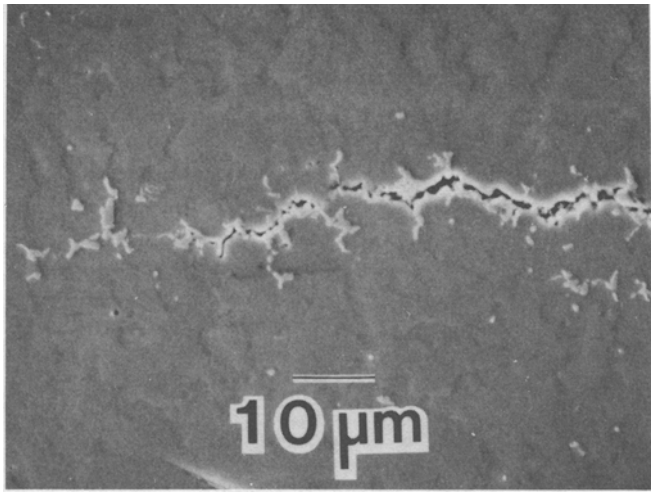

Fig. 3 — SEM micrograph of weld hot-cracked region in HASTELLOY C-276.

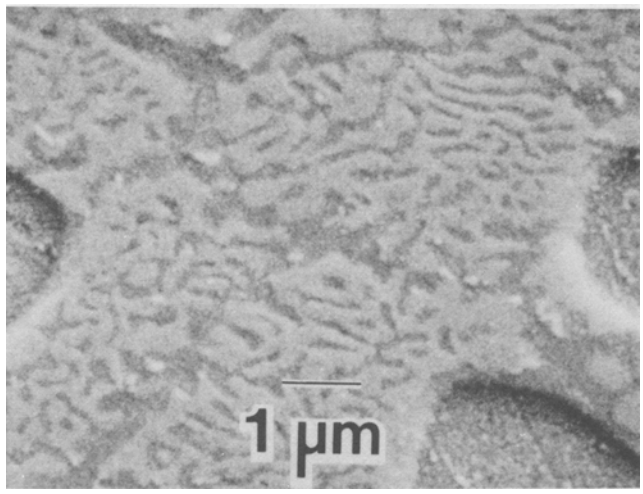

Fig. 6 — SEM micrograph of terminal solidification constituent in INCONEL 718.

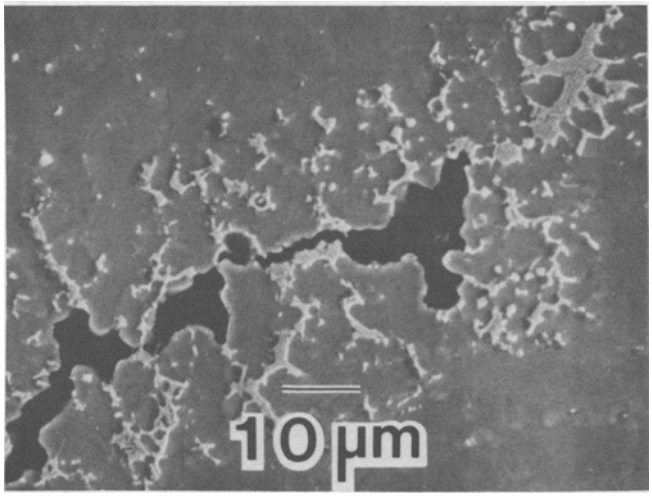

Fig. 4 — SEM micrograph of weld hot-cracked region in INCONEL 625.

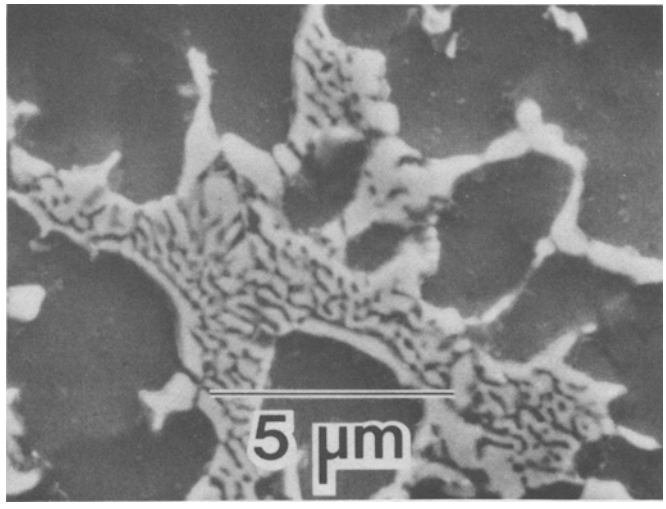

Fig. 7 — SEM micrograph of terminal solidification constituent in INCONEL 625.

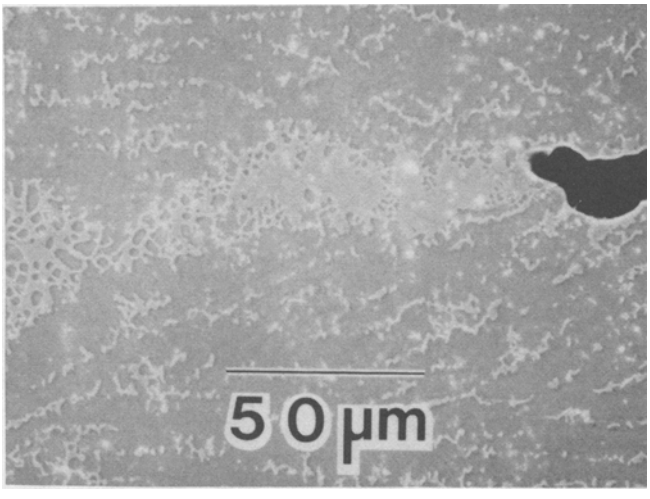

Fig. 5 — SEM micrograph of weld hot-cracked region in INCONEL 718.

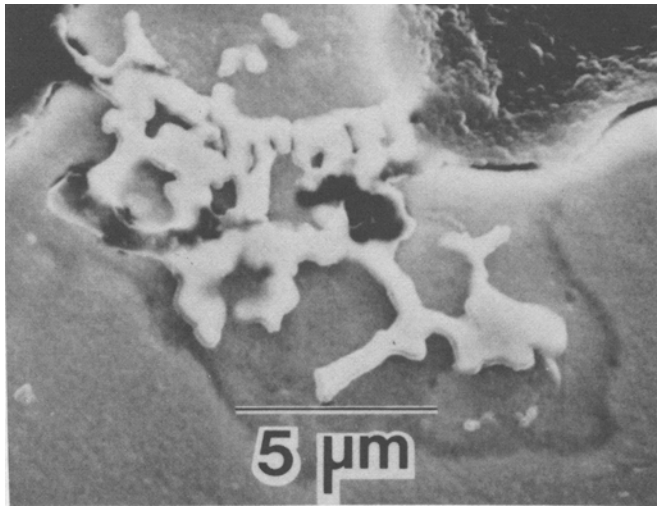

Fig. 8 — SEM micrograph of terminal solidification constituent in HASTELLOY C-22.

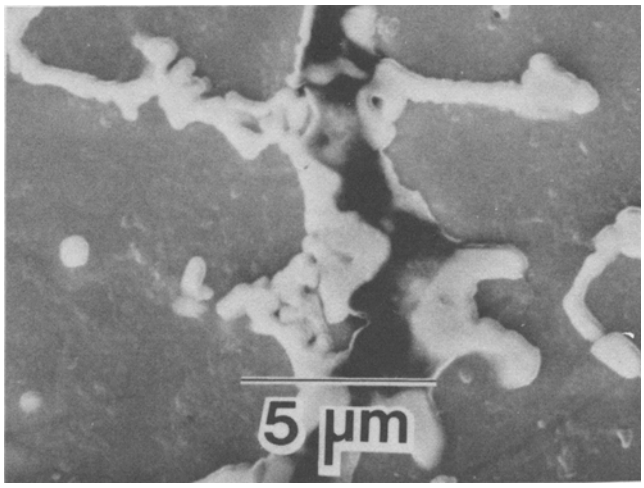

Fig. 9—SEM micrograph of terminal solidification constituent in HASTELLOY C-276.

identified as a Mo-rich σ phase (tetragonal, $a = b = 0.908$ nm, $c = 0.475$ nm). In HASTELLOY C-276, the terminal solidification phase is identified as a Mo-rich P phase (orthorhombic, $a = 0.907$ nm, $b = 1.698$ nm, $c = 0.475$ nm). In the cases of Alloys C-22 and C-276, partial transformation of the terminal solidification constituents to other TCP phases occurs[23,24] on cooling of the weld metal to room temperature. A very small volume fraction of interdendritic TiC is found in HASTELLOY C-4 weld metal.[24] The common microstructural feature found in all of the alloys under study (except HASTELLOY C-4) is the occurrence of a terminal solidification constituent involving a TCP phase.

B. *Segregation and Chemical Effects*

The solidification segregation patterns leading to the formation of these terminal solidification constituents are shown in Figures 10 (a) through (e). All alloys exhibit a depletion of Ni in interdendritic volumes (ID) and an accompanying increase in the concentration of most solute species (Mo, Nb, Ti, *etc.*) in these same regions, especially those having relatively high m_d^i values. The reverse pattern can be seen in dendrite core (DC) regions as must be the case to conserve alloy content.

Ni has a very low m_d^i (Table I), resulting from a relatively full shell of *d*-band electrons, which results in the well-known ability of Ni to accommodate relatively large amounts of alloying components in solid solution. As the alloys under study solidify, the segregation phenomenon shown in Figure 10 causes the instantaneous value of M_d within a dendrite to increase as it grows out from its central spine (DC). This can be seen in Figures 11 (a) through (c), which plots M_d as a function of position within a dendrite. These M_d values are calculated from the compositional profiles given in Figure 10.

IV. DISCUSSION

The formation of interdendritic terminal solidification constituents involving TCP phases is of fundamental importance during the fusion welding of nickel-base alloys. The formation of terminal solidification constituents accompanies an extension of the solidification temperature range. The presence of a liquid phase, from which terminal constituents form at lower temperatures, has been shown by several investigators[28,29,30] to be harmful from a weld hot-cracking standpoint.

Recent work[24,31,32] involving hot-crack testing, differential thermal analysis, and microstructural identification has indicated that even among nickel alloys considered to be readily weldable (HASTELLOYS C-4, C-22, C-276), the presence of a small volume fraction of a terminal solidification constituent involving TCP phases can be detrimental to an alloy's resistance to hot cracking. In several Nb-containing iron-base and nickel-base austenitic alloys, the presence of a Laves phase containing terminal solidification constituent has been shown[32,33,34] to be detrimental to weld metal hot-cracking resistance.

A. *Solidification Considerations*

Secondary solidification constituents form when the terminal solid solubility of an alloy is exceeded. That is, the primary solidification phase (in this case, γ) can no longer accommodate the alloy concentration imposed upon it by solidification segregation. At this point, other phases form from the liquid which are more thermodynamically and structurally capable of absorbing this higher alloy concentration. In the case of Ni-base alloys, several secondary solidification constituents are possible, including carbides, borides, nitrides, γ', and a host of possible intermetallic phases.

With a simple solidification model, Scheil[35] showed how, for a simple binary system, the formation of a eutectic constituent could occur when such a solidification product could not be predicted from the application of equilibrium phase diagram principles. His relationship defining the instantaneous composition of solid forming as a function of the fraction solidified, often referred to as the "non-equilibrium lever rule", is given below,

$$C_s = kC_0(1 - f_s)^{k-1} \qquad [4]$$

where C_s is the instantaneous solid composition forming at any fraction solid, f_s; k is the distribution coefficient for the system, defined as the ratio of the composition of the solid to the composition of the liquid with which it is in equilibrium; and C_0 is the nominal alloy composition. If C_0 is defined in terms of weight percent, then C_s has the units of weight percent and f_s is the weight fraction solidified.

For elements which depress the melting point of a pure metal or alloy, $k < 1$. Application of Eq. [4] for the case of $k < 1$ gives the result that the initial solid to form is depleted in that particular alloying element while the last solid to form is enriched in that same alloying element. This can be seen schematically in Figure 12, which shows a partial binary phase diagram for the hypothetical alloy system, A-B. This eutectic-type system has limited solid solubility of element B in a matrix of element A. When this solubility is exceeded, a TCP second phase forms in the microstructure. This system has a distribution coefficient equal to 0.5, which can be determined by taking the ratio of solidus to liquidus concentrations of element B for any hypoeutectic

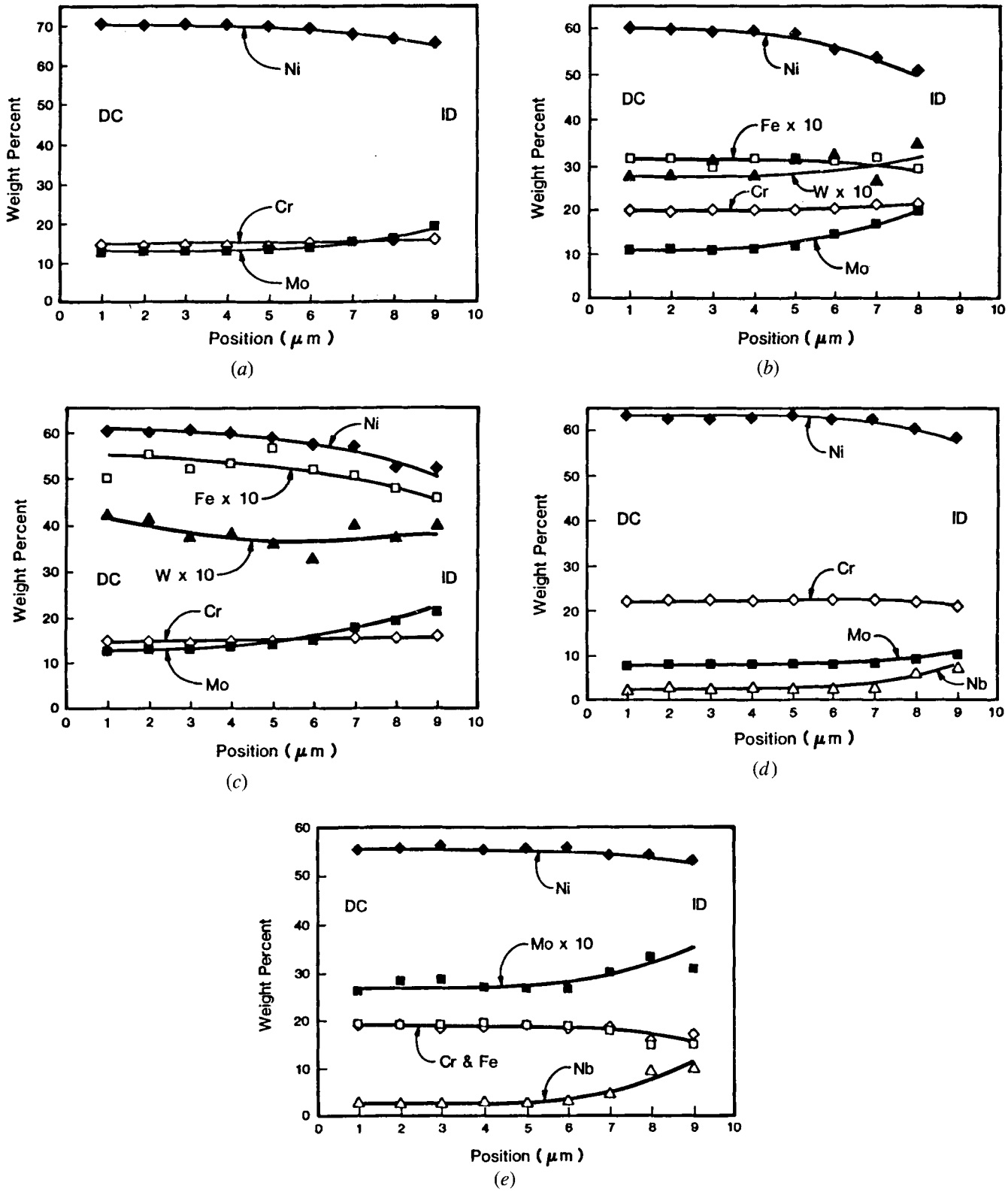

Fig. 10— Weld metal solidification segregation patterns, determined by microprobe, of (*a*) HASTELLOY C-4, (*b*) HASTELLOY C-22, (*c*) HASTELLOY C-276, (*d*) INCONEL 625, and (*e*) INCONEL 718.

composition at all temperatures above the eutectic temperature, T_E. This alloy system has a maximum solid solubility of element B in the γ matrix of $2C_0$. Application of Eq. [4] to an alloy of composition C_0 would result in an initial solid to form at a composition of $0.5C_0$. Subsequent solid compositions would be those defined by the solidus line at temperatures below T_L, also in accordance with Eq. [4]. The terminal solubility of element B in the γ matrix would occur when the solid having a composition of $2C_0$ forms. At this point, the remaining liquid will solidify as the eutectic constituent ($4C_0$), with one of the eutectic phases being the TCP phase. Figure 13 shows graphically the solidification solute profile derived from Eq. [4] for the alloy of composition C_0 given in Figure 12. A reverse pattern of solute element segregation (decreasing C_s with increasing f_s) would occur in the case of $k > 1$.

For the alloy C_0, Eq. [4] predicts that 6.25 wt pct of the microstructure will be composed of the eutectic constituent. In general, less than the predicted amount of eutectic constituent is observed,[36,37] as diffusion in the solid phase during solidification modifies the interfacial solid and liquid compositions toward those defined by equilibrium solidification (*i.e.*, no eutectic constituent formation).

Although this simple model neglects such phenomena as solid-state diffusion during solidification, the effects of undercooling due to interface curvature, and the formation of dendritic side-branching, it is quite useful in illuminating several of the salient features observed during many commercial solidification processes. A similar model has been developed by Bower *et al.*[38] for describing cellular dendritic growth. This model reduces to Eq. [4] in its simplest form and predicts the same pattern for interdendritic segregation as that shown in Figure 13. That is, Eq. [4] predicts the segregation profile expected between the center of a dendrite (dendrite core) and its associated interdendritic region. Examination of the shapes of the solute elements' profiles shown in Figure 10 reveals that they are qualitatively similar to those shown in Figure 13 for the hypothetical case. In addition, the weld metal solidification segregation patterns reported by several investigators[39,40,41] for austenitic stainless steels are also in qualitative agreement with a Scheil-type model (Eq. [4]).

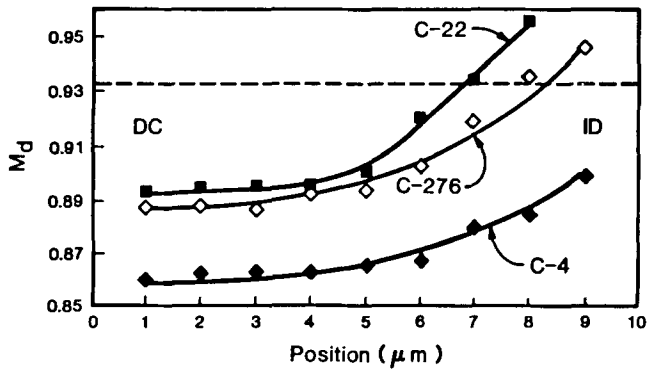

(*a*)

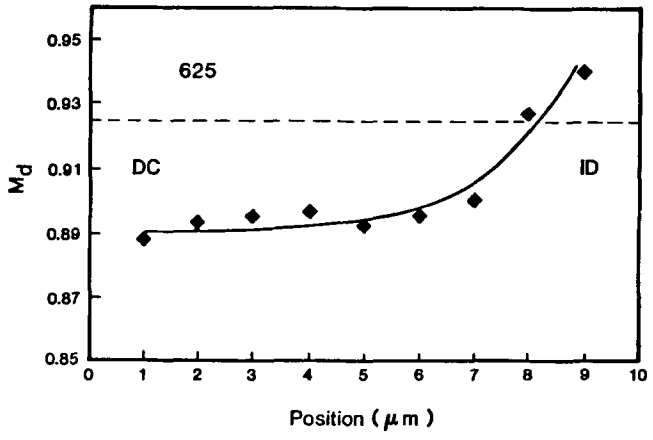

(*b*)

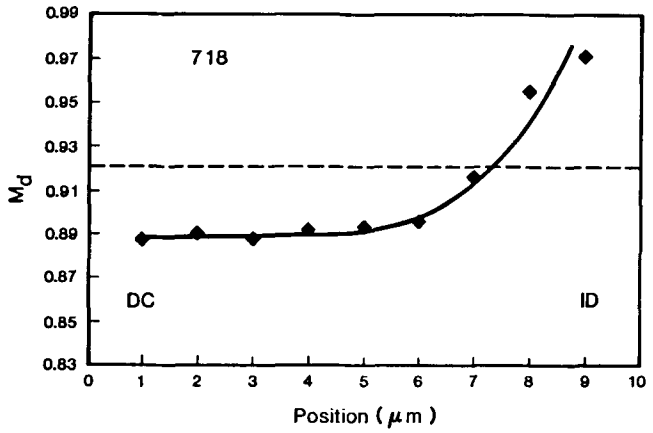

(*c*)

Fig. 11—M_d profiles calculated from the data of Fig. 10; (*a*) HASTELLOYS C-4, C-22, C-276, (*b*) INCONEL 625, and (*c*) INCONEL 718. The dotted line is the M_d^{crit} for the alloy or group of alloys in each figure.

B. *Correlation between Solidification and New PHACOMP*

As can be seen in Figure 13, all compositions between $0.5C_0$ and $2C_0$ are predicted to exist in the solidifying γ dendrite. As stated above, the solid forming immediately

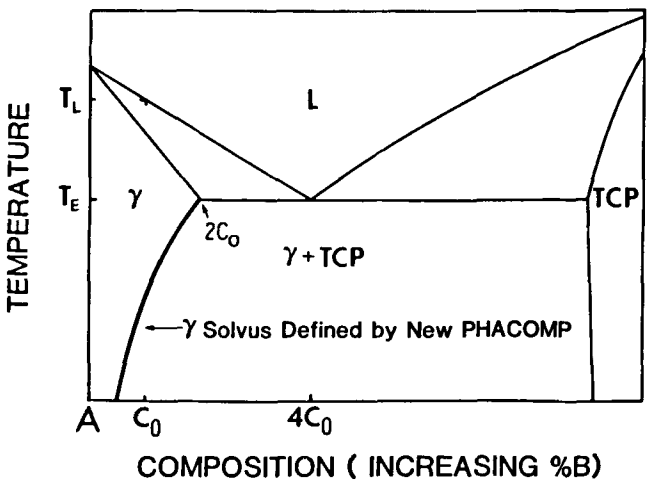

Fig. 12—Hypothetical binary phase diagram of a γ/TCP-type system.

prior to the terminal solidification eutectic constituent has the composition of the maximum solid solubility. In addition to being the locus of the lowest solidus temperature, this concentration represents the top (in terms of temperature) of the γ solvus. This solvus line is the locus of points defined by the temperature-dependent New PHACOMP. The commonality of the maximum solid solubility to both lines (solidus and γ solvus) is the link between New PHACOMP and basic solidification theory. That is, New PHACOMP defines the terminal solid solubility during solidification in the same manner as it defines the γ solvus in the solid state.

It is therefore proposed that the critical values of M_d determined from New PHACOMP calculations can be used to predict the formation of terminal solidification TCP phases in nickel base alloy weldments. Figure 11 shows the M_d profiles calculated from the microprobe chemistry data (Figure 10 data plus the remainder of the minor alloying elements analyzed with the microprobe during this profiling, but not shown in Figure 10) obtained from GTA weld metal. The horizontal dotted line is the critical M_d value for the formation of σ as given by Eq. [3]. The temperature values used as input to Eq. [3] are the secondary solidification (formation of TCP phase-containing constituents) temperatures determined by earlier DTA analyses.[24,31,32] These temperatures are given in Table III. The critical values of M_d are 0.931 for the HASTELLOYS and 0.926 for INCONELS 625 and 718. According to Morinaga *et al.*,[17] the critical M_d value for the formation of Laves phase is lower than for σ phase, while that for P phase would be similar to that for σ phase. In the case where Laves forms (INCONELS 625 and 718), the critical M_d value referenced to σ formation would be an overly conservative test of the application of the New PHACOMP to predicting terminal Laves solidification.

The data of Figure 11 show that terminal solidification involving TCP phases would be predicted (M_d exceeds the critical values in interdendritic regions) by the New PHACOMP calculations for all alloys except HASTELLOY C-4, where the extent of solidification segregation is such that the maximum solid solubility relative to TCP phase formation is not exceeded. These results are in agreement with the SEM and transmission electron microscopy observations in that only HASTELLOY C-4 was devoid of an interdendritic TCP phase. The high Ni content of HASTELLOY C-4 results in a bulk M_d that is lower than that of the other alloys studied. The amount of segregation necessary to initiate TCP phase formation is therefore greater than that for the other alloys studied, and this required segregation does not occur for the welding conditions used in this study.

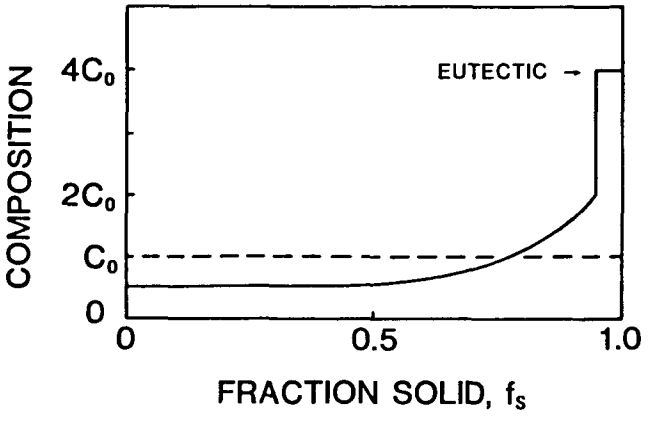

Fig. 13—Plot of the Scheil[35] equation for the alloy C_0 shown in Fig. 12.

In performing the New PHACOMP calculations, it was assumed that no other competing terminal solidification constituents (eutectic carbides, nitrides, borides, *etc.*) were present to accommodate the segregating alloying components. For the alloys under consideration, this was generally true except for the case of INCONEL 718, in which some eutectic NbC was observed. In the case of HASTELLOY C-4, the trace amounts of TiC observed would not have affected the calculations, as the bulk Ti content is low. In more complex superalloys containing substantial amounts of eutectic-type carbides, borides, nitrides, *etc.*, a philosophy similar to that used in applying New PHACOMP to the solid state might be envisioned. That is, a net residual composition could be determined after the contributions of the earlier forming eutectic-type constituents are subtracted.

It becomes clear that the class of alloys to which New PHACOMP may be best applied at the present time to predict terminal TCP phase solidification are those which are not likely to form solidification-type carbides, nitrides, or borides. Although this may seem like a serious limitation to the usefulness of New PHACOMP in this application, it is clear that there are many alloy systems for which it could be directly applicable. In fact, its usefulness may become most apparent in considering the prediction of weld solidification microstructures in dissimilar metal joints, when the net alloy formed by the combination of two different alloys, and maybe even a third alloy as a filler metal, is not itself a well-known or commercial composition.

As described in this paper, the New PHACOMP calculations cannot independently predict *which* TCP phase will occur upon solidification. Even in solid state applications, New PHACOMP does not give a direct prediction of which TCP phase will form in a given alloy. Rather, an available phase diagram, usually of a ternary system which is the closest approximation to a given alloy is referenced to decide which phase may be the most likely to appear. Polar phase diagrams, as described by Sims,[3] have also been used as predictive tools. In cases where alloying elements such as Nb and Ta are present, "size-effect" phases such as Laves can often be expected. A judicious use of available phase diagrams should serve equally well in the present case. For example, in the Ni-Cr-Mo system, it could be expected, based upon available data,[23,24,42] that alloys having a high concentration ratio of Cr to Mo will be likely to form σ as the terminal TCP phase, whereas those alloys having a high concentration ratio of Mo to Cr will form P as the terminal TCP phase.

Table III. DTA Terminal Solidification Temperatures

Alloy	TCP Phase Involved	Temperature (°C)
HASTELLOY C-4	none	—
HASTELLOY C-22	σ	≈1285
HASTELLOY C-276	P	≈1285
INCONEL 625	Laves	≈1200
INCONEL 718	Laves	≈1200

As the formation of terminal solidification constituents generally implies an extension of the solidification temperature range, to a first approximation the presence of predicted TCP solidification constituents would be undesirable from a weld metal hot-cracking standpoint. Weld metal hot cracking, though, is a more complex process, and requires more than simply the presence of a low melting point liquid from which these constituents appear. Sufficient restraint stress is also necessary to initiate hot cracking. Aside from this, the physical properties of the liquid in final solidification volumes (interdendritic and intergranular regions) is important in determining the hot-cracking susceptibility of an alloy. If this liquid has low surface tension, it will tend to spread out as a continuous thin film and increase the propensity toward cracking. On the other hand, if the residual liquid has a high surface tension, it will have a tendency to spheroidize and remain in isolated pockets and the hot-cracking tendency will be diminished. This theory was established by Borland[30] who used it to explain the reduction in hot-cracking tendency imparted by the addition of manganese to mild steels containing sulfur.

More recently, Jolley and Geraghty[43] showed that magnesium additions to Fe-18Cr-13Ni-Nb austenitic stainless steel caused "globularization" of the terminal solidification NbC/austenite eutectic-type constituent, reducing the propensity to hot crack. The ability to predict the formation of a TCP terminal solidification constituent, therefore, is obviously *not* sufficient to predict the hot-cracking behavior of an alloy in a particular situation but rather may serve as an indicator of potential difficulties.

The correlation observed between New PHACOMP calculations and terminal TCP solidification constituents was made through the measurement of solidification segregation patterns. It is clear that for a calculational approach such as this to be effective as a predictive tool, the ability to know these solidification segregation profiles *a priori* is important. This can happen only by incorporating weld solidification modeling into the New PHACOMP analysis. The reality of solid state diffusion during solidification, initially described by Brody and Flemings[36] and recently formulated for weld metal solidification by Brooks,[37] must also be included. For alloys more complex than binary systems, essential input parameters for computational modeling efforts, such as distribution coefficients, are generally unknown, and even less is known experimentally about how interactions between alloying elements can affect the values of these parameters. Generation of a fundamental solidification data base for complex nickel alloys should allow for the successful application of a New PHACOMP type approach to the analysis of weld metal solidification structure. A similar predictive capability should also be possible for austenitic iron base alloys as the quantum mechanical calculations similar to those already made for nickel-rich austenitic alloys are performed for these other systems.

C. *Closure*

Although it is clear that the application of New PHACOMP to predicting solidification behavior is, at the present time, not fully matured, it is equally clear that this new type of approach to predict weld solidification microstructure has merits. In general, any system could be analyzed in this manner as long as the basic calculations for electronic structure[18] are performed and the correlations relative to phase stability are determined. The appeal of this philosophy is in its fundamental nature and its potential application to many multicomponent alloy systems of industrial importance.

V. CONCLUSIONS

1. A variety of nickel base alloys have been found to terminate solidification with the formation of a TCP phase-containing constituent. These constituents are associated with weld metal hot cracks.
2. The solidification segregation pattern observed in all alloys examined was one of Ni depletion and alloy element enhancement in final solidification (interdendritic) volumes.
3. New PHACOMP calculations performed on these segregation profiles revealed a pattern of increasing M_d as one traverses from dendrite core regions to interdendritic volumes.
4. When critical M_d values were exceeded, it was observed that TCP phase-containing terminal solidification constituents were formed. When critical M_d values were not exceeded, no such constituents were observed.
5. It is proposed that the New PHACOMP calculational process can be used as a tool for predicting solidification TCP phases in many nickel base alloys. It may also serve as an indicator of potential weld metal hot-cracking problems in these same alloys.

ACKNOWLEDGMENTS

The authors thank Ms. Ellen Semarge for performing the electron microprobe analyses reported in this paper, Mr. William Hammetter and Mr. Thomas Kollie for performing the DTA tests in the referenced studies, and Mr. Thomas Lienert for assistance with the welding experiments. This work was performed at Sandia National Laboratories, Albuquerque, New Mexico, supported by the United States Department of Energy under contract number DE-AC04-76DP00789.

REFERENCES

1. S. T. Wlodek: *Trans. Am. Soc. Met.*, 1964, vol. 57, pp. 110-19.
2. E. W. Ross: *Journal of Metals*, 1967, vol. 19, No. 12, pp. 12-14.
3. C. T. Sims: *Journal of Metals*, 1966, vol. 18, No. 10, pp. 1119-30.
4. S. T. Wlodek: *Trans. Am. Soc. Met.*, 1963, vol. 56, pp. 287-303.
5. D. K. Das, S. P. Rideout, and P. A. Beck: *Trans. AIME*, 1952, vol. 194, pp. 1071-79.
6. D. S. Bloom and N. J. Grant: *Trans. AIME*, 1953, vol. 197, p. 88.
7. P. Greenfield and P. A. Beck: *Trans. AIME*, 1954, vol. 200, pp. 253-57.
8. P. Greenfield and P. A. Beck: *Trans. AIME*, 1952, vol. 206, pp. 265-75.
9. D. P. Shoemaker, C. B. Shoemaker, and F. C. Wilson: *Acta Crystall.*, 1957, vol. 10, pp. 1-14.
10. L. Pauling: *Physical Review*, Dec. 1, 1938, vol. 54, pp. 899-904.
11. A. H. Sully and T. J. Heal: *Research*, 1948, vol. 1, p. 228.
12. L. R. Woodyatt, C. T. Sims, and H. J. Beattie, Jr.: *Trans. AIME*, 1966, vol. 236, pp. 519-27.
13. C. T. Sims: *The Superalloys*, C. T. Sims and W. C. Hagel, eds., Wiley-Interscience, New York, NY, 1972, p. 276.
14. H. J. Murphy, C. T. Sims, and A. M. Beltran: *Journal of Metals*, 1968, vol. 20, No. 12, pp. 46-54.

15. J. R. Mihalisin, C. G. Bieber, and R. T. Grant: *Trans. AIME*, 1968, vol. 242, pp. 2399-2414.
16. R. G. Barrows and J. B. Newkirk: *Metall. Trans.*, 1972, vol. 3, pp. 2889-93.
17. M. Morinaga, N. Yukawa, H. Adachi, and H. Ezaki: *Superalloys 1984*, pp. 523-32.
18. M. Morinaga, N. Yukawa, and H. Adachi: *J. Phys. Soc. Japan*, 1984, vol. 53, No. 2, pp. 653-63.
19. A. L. Schaefler: *Metal Progress*, 1949, vol. 11, No. 56, pp. 680-80B.
20. C. J. Long and W. T. DeLong: *Welding Journal*, 1973, vol. 52, No. 7, pp. 281s-97s.
21. V. Kujanpaa, N. Suutala, T. Takalo, and T. Moisio: *Welding Research International*, 1979, vol. 9, No. 2, p. 55.
22. D. L. Olson: *Welding Journal*, 1985, vol. 64, No. 10, pp. 281s-95s.
23. M. J. Cieslak, A. D. Romig, Jr., and T. J. Headley: *Microbeam Analysis — 1985*, pp. 179-88.
24. M. J. Cieslak, T. J. Headley, and A. D. Romig, Jr.: *Metall. Trans. A*, 1986, vol. 17A, pp. 2035-47.
25. W. F. Savage and C. D. Lundin: *Welding Journal*, 1965, vol. 44, No. 10, pp. 433s-42s.
26. W. F. Savage and C. D. Lundin: *Welding Journal*, 1966, vol. 45, No. 11, pp. 497s-502s.
27. G. F. Bastin, F. J. J. van Loo, and H. J. M. Heijligers: *X-ray Spec.*, 1984, vol. 13, p. 91.
28. W. I. Pumphrey and P. H. Jennings: *J. Inst. Met.*, 1948, vol. 75, pp. 235-56.
29. W. S. Pellini: *Foundry*, 1952, vol. 80, pp. 124-33, 192, 194, 196, 199.
30. J. C. Borland: *British Welding Journal*, 1960, vol. 7, No. 8, pp. 508-12.
31. M. J. Cieslak, T. J. Headley, and A. D. Romig, Jr.: Sandia National Laboratories, Albuquerque, NM, unpublished research, 1985.
32. G. A. Knorovsky and T. J. Headley: Sandia National Laboratories, Albuquerque, NM, unpublished research, 1985.
33. Y. Nakao, H. Oshige, S. Koga, H. Nishihara, and J. Sugitani: *Jour. Japan Weld. Soc.*, 1982, vol. 51, No. 12, pp. 21-27.
34. R. Vincent: *Acta Metall.*, 1985, vol. 33, No. 7, pp. 1205-16.
35. E. Scheil: *Z. Metallk.*, 1942, vol. 34, p. 70.
36. H. D. Brody and M. C. Flemings: *Trans. AIME*, 1966, vol. 236, pp. 615-23.
37. J. A. Brooks: *66th AWS Convention Abstracts*, Amer. Weld. Soc., 1985, pp. 194-95.
38. T. F. Bower, H. D. Brody, and M. C. Flemings: *Trans. AIME*, 1966, vol. 236, pp. 624-34.
39. Y. Arata, F. Matsuda, and F. Katayama: *Trans. JWRI*, 1977, vol. 6, No. 1, pp. 105-16.
40. M. J. Cieslak, A. M. Ritter, and W. F. Savage: *Welding Journal*, 1982, vol. 61, No. 1, pp. 1s-8s.
41. J. A. Brooks, J. C. Williams, and A. W. Thompson: *Metall. Trans. A*, 1983, vol. 14A, pp. 23-31.
42. D. S. Bloom and N. J. Grant: *Journal of Metals*, 1954, vol. 200, pp. 261-68.
43. G. Jolley and J. E. Geraghty: *Solidification and Casting of Metals*, The Metals Society, London, 1979, pp. 411-15.